

Measurement-Induced Transitions of the Entanglement Scaling Law in Ultracold Gases with Controllable Dissipation

Shimpei Goto* and Ippei Danshita†

Department of Physics, Kindai University, Higashi-Osaka city, Osaka 577-8502, Japan

(Dated: January 13, 2020)

Recent studies of quantum circuit models have theoretically shown that frequent measurements induce a transition in a quantum many-body system, which is characterized by the change of the scaling law of the entanglement entropy from the volume law to the area law. In order to propose a way for experimentally observing this measurement-induced transition, we present numerical analyses using matrix-product states on quench dynamics of a dissipative Bose-Hubbard model with controllable two-body losses, which has been realized in recent experiments with ultracold atoms. We find that when the strength of dissipation increases, a measurement-induced transition occurs in a region of relatively small dissipation. We also find that the strong dissipation leads to a revival of the volume-law scaling due to a continuous quantum Zeno effect. We show that three different states appearing in the measurement-induced transitions can be distinguished by measuring the momentum distribution.

In a generic quantum many-body system, a pure state is thermalized via long-time evolution, i.e., its expectation values of local observables are very close to those given by a statistical (micro-) canonical ensemble [1–3]. The entanglement entropy of such a thermal pure state obeys volume-law scaling, corresponding to the fact that the entropy of a thermal density matrix is extensive [4–6]. Recent advances in understanding and controlling coherent quantum many-body dynamics have revealed a few exceptional systems which do not show such thermalization. First, in integrable systems, such as the Lieb-Liniger model and the Ising model with a transverse field, many integrals of motion prevent a pure state from relaxation towards a thermal state [1, 7–9]. Second, in many-body localized (MBL) systems, disordered potentials forbid ballistic propagation of quantum information such that the entanglement entropy grows only logarithmically with time [2, 3, 10, 11].

Recent theoretical studies of quantum circuit models have proposed another class of exceptional systems [12–21]. In these studies, random unitary dynamics with probabilistic measurements have been investigated. It has been shown that when the probability of measurements increases, the scaling law of the entanglement entropy exhibits a transition from the volume law to the area law at a certain critical point. Since the volume-law scaling is a necessary condition for a pure state to be thermal, the emergence of the area-law state means that many measurements prevent a state after long-time evolution from the thermalization. Despite the intensive interest in this measurement-induced transition, its experimental observation is still lacking. This is mainly because at present the number of available qubits, which must be free from uncontrolled decoherence, in quantum circuit systems is not large enough to observe the transition.

Ultracold gases have served as an ideal platform for analyzing long-time coherent dynamics of many-body sys-

tems thanks to their long thermalization time and isolation from the environment. Indeed, coherent quantum dynamics of integrable systems [7] and MBL systems [22] have been observed in this platform for the first time. Recent experiments have successfully introduced controllable dissipation to ultracold-gas systems to create and manipulate quantum many-body states [23–27]. Since the introduced dissipation corresponds to a continuous quantum measurement, which can be interpreted as probabilistic measurements in terms of quantum trajectory representation of open quantum systems, we expect that it may be utilized for causing the measurement-induced transition.

In this Letter, we propose a specific protocol to realize the measurement-induced transition with use of ultracold gases in optical lattices. By means of the quantum trajectory method implemented with matrix product states (MPS) [28–30], we analyze the one-dimensional (1D) Bose-Hubbard model with two-body losses, which can be widely controlled in experiment by the strength of a photoassociation (PA) laser [26]. We find that this system exhibits a measurement-induced transition when the strength of the two-body losses increases in a weakly dissipative regime. Moreover, we find another transition in a strongly dissipative regime. The latter transition can be attributed to a continuous quantum Zeno effect (QZE) and has not been reported in previous literature studying quantum circuit models. We show that a characteristic feature of the intermediate area-law state emerges as the dips at $|k| = \pi/(2d)$ in the momentum distribution, where d is the lattice spacing.

Model and methods.— We consider ultracold bosons confined in an optical lattice. We assume that the lattice potential in the transverse (yz) directions is so deep that the hopping in these direction is forbidden, i.e., the system is 1D. We also assume that the lattice potential in the longitudinal (x) direction is deep enough for the tight-binding approximation to be valid. The two-body

losses can be introduced by exposing the system to a PA laser [26], which couples a local two-atom state to a molecular state with a very short lifetime. In this system, the time-evolution of a density matrix $\hat{\rho}(t)$ can be effectively described by the master equation in Lindblad form [26, 31, 32]

$$\frac{d}{dt}\hat{\rho}(t) = -\frac{i}{\hbar}[\hat{H}, \hat{\rho}(t)] + \hat{L}[\hat{\rho}(t)] \quad (1)$$

with the 1D Bose-Hubbard Hamiltonian

$$\hat{H} = -J \sum_{i=1}^{M-1} (\hat{b}_i^\dagger \hat{b}_{i+1} + \text{H.c.}) + \frac{U}{2} \sum_{i=1}^M \hat{n}_i (\hat{n}_i - 1), \quad (2)$$

and the Lindblad superoperator for two-body atom losses

$$\hat{L}[\hat{\rho}] = -\frac{\gamma}{2} \sum_i (\hat{b}_i^\dagger \hat{b}_i^\dagger \hat{b}_i \hat{\rho} + \hat{\rho} \hat{b}_i^\dagger \hat{b}_i^\dagger \hat{b}_i \hat{b}_i - 2\hat{b}_i \hat{b}_i \hat{\rho} \hat{b}_i^\dagger \hat{b}_i^\dagger). \quad (3)$$

Here, J is the hopping amplitude, M is the number of lattice sites, \hat{b}_i^\dagger (\hat{b}_i) creates (annihilates) a boson at site i , U is the on-site Hubbard interaction we set $U/J = 5.0$ in this study, $\hat{n}_i = \hat{b}_i^\dagger \hat{b}_i$, and γ is the strength of the two-body inelastic collision which can be controlled by the intensity of the PA laser. Hereafter, we set the lattice spacing $d = 1$ and denote the number of particles remained in the system as N , i.e., $N = \sum_i \langle \hat{n}_i \rangle$. At initial time $t = 0$, we assume that the system is a Mott insulating state at unit filling, i.e., $|\psi_0\rangle = \prod_i \hat{b}_i^\dagger |0\rangle$ and thus $\hat{\rho}(0) = |\psi_0\rangle \langle \psi_0|$, where $|0\rangle$ denotes the vacuum state.

Solving the master equation (1) requires very high numerical cost in general because the number of coefficients in the density matrix is the square of the dimension of the Hilbert space. To circumvent this difficulty, we use quantum trajectory techniques which treat pure states in the density matrix [28, 29] instead of treating the density matrix directly. Following the quantum trajectory techniques, we calculate the time-evolved state

$$|\psi(t)\rangle = e^{-i\frac{t}{\hbar}\hat{H}_{\text{eff}}} |\psi_0\rangle \quad (4)$$

with the effective non-hermitian Hamiltonian

$$\hat{H}_{\text{eff}} = \hat{H} - i\frac{\hbar\gamma}{2} \sum_i \hat{b}_i^\dagger \hat{b}_i^\dagger \hat{b}_i \hat{b}_i. \quad (5)$$

As time t increases, the norm of the time-evolved state $|\psi(t)\rangle$ decreases because of the non-hermitian part of the effective Hamiltonian \hat{H}_{nh} . When the squared norm of the time-evolved state becomes lower than a random number generated from the uniform distribution $(0, 1)$, we calculate a probability $p_i \propto \langle \psi(t) | \hat{b}_i^\dagger \hat{b}_i^\dagger \hat{b}_i \hat{b}_i | \psi(t) \rangle$ and choose one index j according to the probability p_i . Then, the jump operator $\hat{b}_j \hat{b}_j$ is applied to $|\psi(t)\rangle$ and the state is normalized. This stochastic process emulates the open dynamics described by the master equation in Lindblad

form, and the expectation values are obtained by the sample average

$$\begin{aligned} \langle \hat{O}(t) \rangle &= \text{Tr}[\hat{O}\hat{\rho}(t)] \\ &\simeq \frac{1}{K} \sum_{l=1}^K \frac{\langle \psi_l(t) | \hat{O} | \psi_l(t) \rangle}{\langle \psi_l(t) | \psi_l(t) \rangle}, \end{aligned} \quad (6)$$

where $|\psi_l(t)\rangle$ is the l -th sample of the stochastic process and K is the number of samples. For numerically efficient calculations in 1D, we represent states $|\psi(t)\rangle$ with MPS and perform the time evolution by means of the time-evolving block decimation algorithm [33–36] using the optimized Forest-Ruth-like decomposition [37]. Truncation error is set to 10^{-8} , and the time step Δt is adaptively changed after each jump operation as $\Delta t = \min\{-\log(0.9)\hbar / \langle \psi(t) | i\hat{H}_{\text{nh}} | \psi(t) \rangle, \Delta t_{\text{max}}\}$ in order to avoid a rapid decrease in the norm of wavefunction. Here, Δt_{max} is the upper bound of the time step we set to $0.05\hbar/J$ ($0.02\hbar/J$) for small to intermediate γ (large $\hbar\gamma/J \geq 100$).

With this method, we calculate the momentum distribution

$$\langle \hat{n}_k \rangle = \frac{1}{M} \sum_{ij} \langle \hat{b}_i^\dagger \hat{b}_j \rangle e^{-ik(i-j)}, \quad (7)$$

which is a standard observable in ultracold-gas experiments, and the ‘‘entanglement entropy’’. It should be cautioned that we have to define what we call ‘‘entanglement entropy’’ in this study because the ordinary entanglement entropy is defined only for pure states $|\phi\rangle$ on a system biparted into subsystems A and B as

$$S_A(t) = -\text{Tr} \hat{\rho}_A(t) \ln \hat{\rho}_A(t), \quad (8)$$

where $\hat{\rho}_A$ is a reduced density matrix defined as

$$\hat{\rho}_A(t) = -\text{Tr}_B |\phi(t)\rangle \langle \phi(t)|. \quad (9)$$

Here, Tr_B means a partial trace over the subsystem B . In this study, as well as other studies investigating the measurement-induced transition, the statistical average of the entanglement entropy of $|\psi(t)\rangle / \sqrt{\langle \psi(t) | \psi(t) \rangle}$ is called ‘‘entanglement entropy’’ and the size dependence of ‘‘entanglement entropy’’ is discussed. In other words, what we discuss is the typical behavior of the entanglement entropy of relevant states in a density matrix $\hat{\rho}(t)$. An equal bipartition does not always give the maximal entanglement entropy in the presence of the two-body loss. Therefore, we define the average of the maximal bipartite entanglement entropy

$$S_{\text{max}}(t) = \left\langle \max_A S_A(t) \right\rangle, \quad (10)$$

where \max_A means the biparted subsystem A that gives the maximal entanglement entropy. In this study, we discuss the scaling law of the ‘‘entanglement entropy’’ based

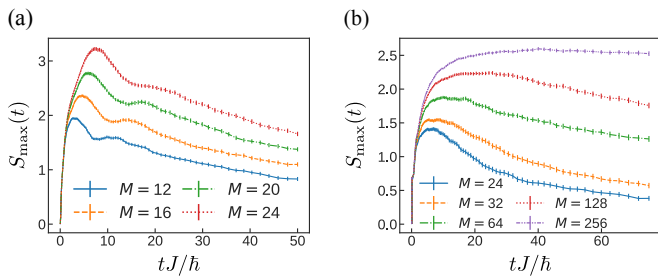


FIG. 1. Time evolution of the entanglement entropy for (a) $\hbar\gamma/J = 0.5$ and (b) $\hbar\gamma/J = 5.0$ for several system sizes. Error bars indicate 1σ uncertainty.

on $S_{\max}(t)$. Hereafter, we call $S_{\max}(t)$ as entanglement entropy for simplicity.

It is worth noting that the measurement-induced transition in the Bose-Hubbard model (2) with local projective measurements has been studied in Ref. [21]. In contrast to the previous study, here we incorporate the specific form of controllable dissipation that has been experimentally realized and show an observable suited for characterizing the transitions.

Measurement-induced transitions in the dissipative Bose-Hubbard models.— Figure 1 shows the time-evolution of the entanglement entropy for different values of $\hbar\gamma/J$ and M . By comparing the case of $(\hbar\gamma/J, M) = (0.5, 24)$ with that of $(\hbar\gamma/J, M) = (5.0, 24)$, we see that the dissipation suppresses the growth of the entanglement entropy. Thanks to this suppression, when $\hbar\gamma/J = 5.0$, we can compute long-time dynamics of a relatively large system, say $N = 256$. The general tendency of the entanglement entropy in the presence of the two-body losses is that it rapidly grows in a short time regime and gradually decreases due to the two-body losses after taking a maximal value. Despite the gradual decrease, we see that a steady-value region, where $S_{\max}(t)$ takes almost a constant value, develops when the system size increases (see, e.g., the region $15 \lesssim tJ/\hbar \lesssim 30$ in the case of $(\hbar\gamma/J, M) = (5.0, 128)$). In the following, we show that a state in the steady-value region obeys the area-law scaling of the entanglement entropy such that we interpret it as an area-law state in the realm of the measurement-induced transition.

Figure 2 shows the maximal values of the entanglement entropy, $\max_t S_{\max}(t)$, during the time evolution as a function of the system size M for $\hbar\gamma/J = 0.5, 5.0, 50.0$, and 500.0 . When the dissipation is as small as $\hbar\gamma/J = 0.5$ or is as large as $\hbar\gamma/J = 500.0$, the entanglement entropy grows linearly with M within the system size that we can numerically compute ($M \simeq 24$), i.e., it follows the volume-law scaling. On the contrary, in an intermediate dissipation regime, including $\hbar\gamma/J = 5.0$ and 50.0 , the entanglement entropy grows logarithmically with M , i.e., it follows the area-law scaling. This means that when the strength of the dissipation increases, the

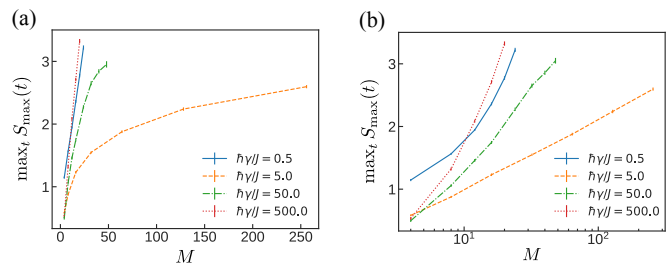


FIG. 2. System size M dependence of the maximal entanglement entropy $\max_t S_{\max}(t)$ (a) in the linear scale for M and (b) in the logarithmic scale for M . The blue solid, orange dashed, green dashed-dotted, and red dotted lines correspond to $\hbar\gamma/J = 0.5, 5.0, 50.0$, and 500.0 , respectively. Error bars indicate 1σ uncertainty.

system exhibits a transition from a volume-law state to an area-law state at a relatively small dissipation and the other transition to another volume-law state at a relatively large dissipation. In short, in the present system the measurement-induced transition has the reentrant structure.

The presence of the volume-law state at the small dissipation, $\hbar\gamma/J = 0.5$, implies that there is a finite critical value $(\hbar\gamma/J)_c$ for the measurement-induced transition likewise the cases of random unitary circuits. On the other hand, that at the large dissipation, $\hbar\gamma/J = 500.0$, can be interpreted as a consequence of the continuous QZE. More specifically, the strong two-body losses suppress double occupation at each site such that the particles in the system behave as hardcore bosons [38]. Hence, after several loss events at an early time range, which create a considerable number of holes, the measurement events rarely happen so that the holes spread ballistically to lead to the volume-law entanglement.

Momentum distribution.— In closed systems, a kind of the entanglement entropy, namely the 2nd order Rény entropy, has been observed in experiments with ultracold gases in optical lattices by preparing a copy of the target system and measuring interference between the target and the copy [39, 40]. However, in open systems with dissipation, it is hard to use the same protocol because the copy cannot perfectly mimic measurement events which happen in a stochastic manner. Hence, it is imperative to point out alternative experimental observables that can discriminate the three types of state appearing in the measurement-induced transitions. We show below that the momentum distribution, which is easily accessible in typical experiments with ultracold gases, is such an observable.

Figure 3 shows the normalized momentum distributions for $\hbar\gamma/J = 0.5, 5.0, 50.0$, and 500.0 at the time that gives $\max_t S_{\max}(t)$. The system size is set to $M = 20$ in order to compute states with the volume-law entanglement. In each of the three different regions of the dissipation strength, $\langle \hat{n}_k \rangle / N$ exhibits a distinct signal. In the

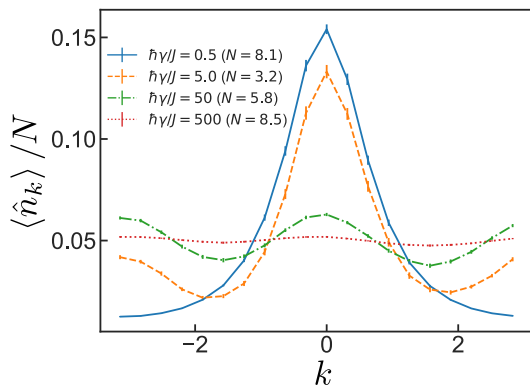


FIG. 3. Normalized momentum distributions for several values of the dissipation strength γ at the time that gives $\max_t S_{\max}(t)$. The blue solid, orange dashed, green dashed-dotted, and red dotted lines correspond to $\hbar\gamma/J = 0.5, 5.0, 50.0,$ and 500.0 , respectively. The system size M is set to 20 in order to investigate a vast range of γ . Error bars indicate 1σ uncertainty.

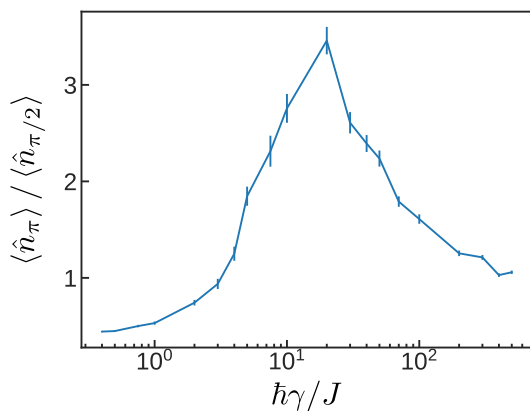


FIG. 4. Visibility $\langle \hat{n}_\pi \rangle / \langle \hat{n}_{\pi/2} \rangle$ as a function of the dissipation strength γ . Although it is in practice impossible to precisely determine the critical points with our MPS method, we have checked that the states in the region $2 \leq \hbar\gamma/J \leq 50$ safely obey the area-law scaling. Error bars indicate 1σ uncertainty.

case of the small dissipation, $\hbar\gamma/J = 0.5$, there exists a single peak at $k = 0$. In the intermediate region, including $\hbar\gamma/J = 5.0$ and 50.0 , the dips at $|k| = \pi/2$ are developed. In the case of the strong dissipation, $\hbar\gamma/J = 500.0$, the distribution is almost flat. In order to characterize the signals more quantitatively, we show in Fig. 4 the visibility $\langle \hat{n}_\pi \rangle / \langle \hat{n}_{\pi/2} \rangle$ as a function of $\hbar\gamma/J$. Since the visibility becomes considerably large in the intermediate region, where the area-law states emerge, it can be used for distinguishing the area-law states from the volume-law states. Notice that the visibility at $M = 20$ shown in Fig. 4 does not exhibit any singular behaviors across the transition points because the system size is too small.

The emergence of the dip structure in the intermediate region can be understood as a QZE in the momentum space. At $t = 0$, there is no doubly-occupied site as de-

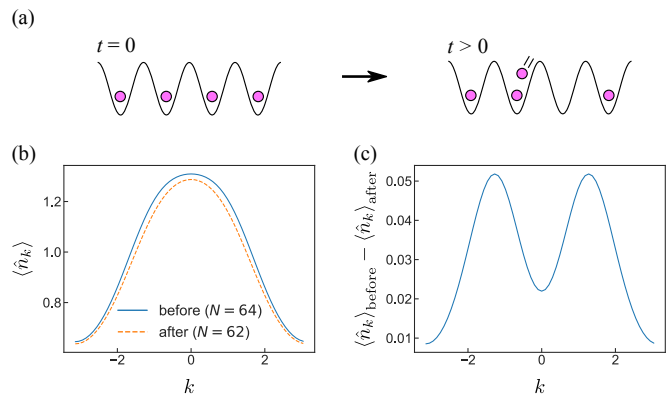


FIG. 5. (a) A possible loss process in the early time dynamics. Atoms with finite group velocity tend to be lost. (b) Momentum distributions before (blue solid line) and after (orange dashed line) a loss event in the early time dynamics. (c) Difference of momentum distributions before and after the loss event. To obtain the momentum distributions, we set $M = 64$.

picted in Fig. 5 (a). This means that in order for the loss events to happen, particles have to move with finite group velocity. In other words, the loss event is more probable for faster particles. Since the group velocity is the largest at $|k| = \pi/2$ in the single-particle band of the 1D Bose-Hubbard model, which is $-2J \cos k$, the particles with $|k| = \pi/2$ is the most likely to be lost. In Figs. 5 (b) and (c), we compare the momentum distribution right before and after a loss event during early-time dynamics and see that the momentum distribution of the lost two particles is indeed peaked at $|k| = \pi/2$. As a consequence of series of such loss events, $\langle \hat{n}_k \rangle / N$ forms the dips at $|k| = \pi/2$. After the formation of the dip structure, the stronger dissipation for faster particles suppresses the redistribution of the particles towards states around $|k| = \pi/2$.

Summary.— We proposed the measurement-induced transitions, which have been theoretically found in recent studies of quantum circuit models [12–21], can be experimentally observed by using ultracold bosons in optical lattices with controllable dissipation. We employed a quasi-exact numerical method to investigate effects of dissipation on quench dynamics of the one-dimensional Bose-Hubbard model with a two-body loss term. By comparing the maximal entanglement entropy of the system during the time evolution, we found two measurement-induced transitions. Specifically, when the strength of the dissipation increases, the scaling of the entanglement changes from the volume law to the area law, and again to the volume law. We showed that the momentum distribution provides a signal for distinguishing the three different regions.

We could not locate precisely the critical points for the two measurement-induced transitions because it was impossible to efficiently describe the volume-law states of the dissipative Bose-Hubbard model with currently

available numerical techniques. Since experiments with ultracold gases do not suffer from the volume-law entanglement, the determination of the critical points will be a meaningful target of quantum simulations.

We thank S. Nakajima, Y. Takahashi, Y. Takasu, and T. Tomita for fruitful discussions. The MPS calculations in this work are performed with ITensor library, <http://itensor.org>. This work was financially supported by KAKENHI from Japan Society for the Promotion of Science: Grant No. 18K03492 and No. 18H05228, by CREST, JST No. JPMJCR1673, and by MEXT Q-LEAP Grant No. JPMXS0118069021.

* goto@phys.kindai.ac.jp

† danshita@phys.kindai.ac.jp

- [1] M. Rigol, V. Dunjko, and M. Olshanii, *Nature* **452**, 854 (2008).
- [2] R. Nandkishore and D. A. Huse, *Annu. Rev. Condens. Matter Phys.* **6**, 15 (2015), arXiv:1404.0686.
- [3] D. A. Abanin, E. Altman, I. Bloch, and M. Serbyn, *Rev. Mod. Phys.* **91**, 021001 (2019).
- [4] J. Eisert, M. Cramer, and M. B. Plenio, *Rev. Mod. Phys.* **82**, 277 (2010).
- [5] Y. O. Nakagawa, M. Watanabe, H. Fujita, and S. Sug-iura, *Nat Commun* **9**, 1 (2018).
- [6] J. R. Garrison and T. Grover, *Phys. Rev. X* **8**, 021026 (2018).
- [7] T. Kinoshita, T. Wenger, and D. S. Weiss, *Nature* **440**, 900 (2006).
- [8] M. Rigol, V. Dunjko, V. Yurovsky, and M. Olshanii, *Phys. Rev. Lett.* **98**, 050405 (2007).
- [9] L. Vidmar and M. Rigol, *J. Stat. Mech.* **2016**, 064007 (2016).
- [10] M. Žnidarič, T. Prosen, and P. Prelovšek, *Phys. Rev. B* **77**, 064426 (2008).
- [11] J. H. Bardarson, F. Pollmann, and J. E. Moore, *Phys. Rev. Lett.* **109**, 017202 (2012).
- [12] Y. Li, X. Chen, and M. P. A. Fisher, *Phys. Rev. B* **98**, 205136 (2018).
- [13] A. Chan, R. M. Nandkishore, M. Pretko, and G. Smith, *Phys. Rev. B* **99**, 224307 (2019).
- [14] B. Skinner, J. Ruhman, and A. Nahum, *Phys. Rev. X* **9**, 031009 (2019).
- [15] M. Szyniszewski, A. Romito, and H. Schomerus, *Phys. Rev. B* **100**, 064204 (2019).
- [16] C.-M. Jian, Y.-Z. You, R. Vasseur, and A. W. W. Ludwig, *ArXiv190808051 Cond-Mat Physicsquant-Ph* (2019), arXiv:1908.08051 [cond-mat, physics:quant-ph].
- [17] M. J. Gullans and D. A. Huse, *ArXiv190505195 Cond-Mat Physicsquant-Ph* (2019), arXiv:1905.05195 [cond-mat, physics:quant-ph].
- [18] Y. Li, X. Chen, and M. P. A. Fisher, *Phys. Rev. B* **100**, 134306 (2019).
- [19] S. Choi, Y. Bao, X.-L. Qi, and E. Altman, *ArXiv190305124 Cond-Mat Physicshep-Th Physicsquant-Ph* (2019), arXiv:1903.05124 [cond-mat, physics:hep-th, physics:quant-ph].
- [20] Y. Bao, S. Choi, and E. Altman, *ArXiv190804305 Cond-Mat Physicshep-Th Physicsquant-Ph* (2019), arXiv:1908.04305 [cond-mat, physics:hep-th, physics:quant-ph].
- [21] Q. Tang and W. Zhu, *ArXiv190811253 Cond-Mat* (2019), arXiv:1908.11253 [cond-mat].
- [22] M. Schreiber, S. S. Hodgman, P. Bordia, H. P. Lüschen, M. H. Fischer, R. Vosk, E. Altman, U. Schneider, and I. Bloch, *Science* **349**, 842 (2015).
- [23] G. Barontini, R. Labouvie, F. Stubenrauch, A. Vogler, V. Guarrera, and H. Ott, *Phys. Rev. Lett.* **110**, 035302 (2013).
- [24] Y. S. Patil, S. Chakram, and M. Vengalattore, *Phys. Rev. Lett.* **115**, 140402 (2015).
- [25] H. P. Lüschen, P. Bordia, S. S. Hodgman, M. Schreiber, S. Sarkar, A. J. Daley, M. H. Fischer, E. Altman, I. Bloch, and U. Schneider, *Phys. Rev. X* **7**, 011034 (2017).
- [26] T. Tomita, S. Nakajima, I. Danshita, Y. Takasu, and Y. Takahashi, *Sci. Adv.* **3**, e1701513 (2017).
- [27] R. Bouganne, M. B. Aguilera, A. Ghermaoui, J. Beugnon, and F. Gerbier, *Nat. Phys.* **16**, 21 (2020).
- [28] R. Dum, A. S. Parkins, P. Zoller, and C. W. Gardiner, *Phys. Rev. A* **46**, 4382 (1992).
- [29] A. J. Daley, *Adv. Phys.* **63**, 77 (2014), arXiv:1405.6694.
- [30] U. Schollwöck, *Annals of Physics* **326**, 96 (2011).
- [31] V. Gorini, A. Kossakowski, and E. C. G. Sudarshan, *Journal of Mathematical Physics* **17**, 821 (1976).
- [32] G. Lindblad, *Commun.Math. Phys.* **48**, 119 (1976).
- [33] G. Vidal, *Phys. Rev. Lett.* **91**, 147902 (2003).
- [34] G. Vidal, *Phys. Rev. Lett.* **93**, 040502 (2004).
- [35] S. R. White and A. E. Feiguin, *Phys. Rev. Lett.* **93**, 076401 (2004).
- [36] A. J. Daley, C. Kollath, U. Schollwöck, and G. Vidal, *J. Stat. Mech.* **2004**, P04005 (2004).
- [37] I. P. Omelyan, I. M. Mryglod, and R. Folk, *Computer Physics Communications* **146**, 188 (2002).
- [38] J. J. García-Ripoll, S. Dürr, N. Syassen, D. M. Bauer, M. Lettner, G. Rempe, and J. I. Cirac, *New J. Phys.* **11**, 013053 (2009).
- [39] R. Islam, R. Ma, P. M. Preiss, M. Eric Tai, A. Lukin, M. Rispoli, and M. Greiner, *Nature* **528**, 77 (2015).
- [40] A. M. Kaufman, M. E. Tai, A. Lukin, M. Rispoli, R. Schittko, P. M. Preiss, and M. Greiner, *Science* **353**, 794 (2016).